Mechanism of Fe impurity motivated ion-nanopatterning of Si (100) surfaces

Jing Zhou and Ming Lu*
Department of Optical Science and Engineering, Key Laboratory of Micro and Nano Photonic Structures, China Ministry of Education, Fudan University, Shanghai 200433, China
(Received 27 April 2010; revised manuscript received 12 July 2010; published 2 September 2010)

A continuum model is developed to describe surface evolution of Si (100) during normal incidence ion sputtering with Fe incorporation. The model integrates curvature-dependent erosion (CDE), ballistic smoothing, and ion-enhanced viscous flow as the surface processes during ion sputtering without Fe. And it integrates surface stress and preferential sputtering as the effects of Fe incorporation. According to our model, in the presence of Fe, the surface stress-induced instability together with CDE overcomes ballistic smoothing, leading to dot pattern formation in morphology. In addition, preferential sputtering, cooperating with the morphological instability, accomplishes the patterning in composition. The simulations based on this model qualitatively reproduce Fe motivated ion patterning and the surface evolution of prepatterned Si (100) during postsputtering.

DOI: 10.1103/PhysRevB.82.125404 PACS number(s): 81.16.Rf, 68.35.Fx, 79.20.Rf, 81.40.Wx

I. INTRODUCTION

Ion-sputtering-induced nanopatterning of solid surfaces has received considerable attention for its effectiveness in producing ordered nanostructures in a well-controlled manner.[1–6] On the other hand, fabrication of Si nanostructures has long been a subject under investigation due to its potential applications in the development of future optoelectronics.[7–12] The formation mechanism has been described theoretically by the competition between the surface instability and surface relaxation process.[13–16] However, recently it shows that metal incorporation during ion sputtering may influence pattern formation. Ozaydin *et al.*[17] reported that molybdenum incorporation triggers the formation of ordered dot arrays on Si surfaces under the bombardment of Ar^+ ions at normal incidence while no correlated structures are generated in the absence of the impurities. Hofsäss and Zhang[18] found that codeposition of Au, Ag, and Pt surfactants generates novel patterns and nanostructures on Si surfaces during ion sputtering, which are absent without the surfactants. Sanchez-Garcia *et al.*[19] observed a transition from hole to dot pattern on Si by tuning the amount of metal incorporation during ion sputtering at normal incidence. Macko *et al.*[20] observed a variety of patterns on Si surface under ion bombardment with simultaneous sputter deposition of stainless steel. Zhou *et al.*[21] observed dot patterning in both morphology and composition of Si (100) surfaces during ion sputtering with Fe incorporation but only surface smoothing in the absence of Fe. These findings add a new aspect to the present understanding of surface morphology evolution during ion sputtering and suggest modeling studies to describe these phenomena.

In this contribution, a continuum model is developed to describe surface evolution of Si (100) during normal incidence Ar^+ ion sputtering with Fe incorporation. This model, expressed as a coupled two-field equation, describes both morphology and composition evolution by integrating a number of relevant mechanisms. Among these mechanisms, surface stress and preferential sputtering, as two possible effects of Fe incorporation, originate dot patterning. In our model, the surface stress induces patterning in morphology by competing with smoothing mechanisms. Preferential sputtering, cooperating with the surface stress-induced instability, accomplishes patterning in composition. The numerical simulations based on the model qualitatively reproduce Fe motivated ion patterning and the surface evolution of prepatterned Si (100) during postsputtering without Fe.

II. A CONTINUUM MODEL

Modeling of ion-induced surface nanopatterning was pioneered by Bradley and Harper (BH)[13] on the basis of the sputter theory of Sigmund.[22] They explained the formation of periodic patterns as a result of competition between the surface instability induced by curvature-dependent erosion (CDE) and thermal surface diffusion. Later, the BH model was extended into nonlinear regime[14–16,23,24] to explain more experimental features, such as the amplitude saturation. However, all these models are not applicable to describe Fe incorporated Si surface nanopatterning since the metal impurity effect is not included. Recently, Shenoy *et al.*[25] proposed a model to describe sputtering of alloy surfaces, which describes the evolution of both surface height and composition. In this work, we develop a continuum model which integrates a number of surface processes relevant to Fe incorporated ion patterning.

Ion sputtering of Si (100) surface with Fe incorporation is depicted in Fig. 1. A beam of Ar^+ ions is incident normally onto the surface with a uniform flux of F. Fe atoms are codeposited onto the surface at a constant rate. Due to cascade collision and ion mixing, an altered surface layer is formed during sputtering. In the following, we restrict our attention to this layer and assume that all the surface processes relevant to ion patterning take place in this layer. For steady state sputtering of a planar surface, the surface layer thickness Δ, and compositions c_{Si} and $c_{Fe}=1-c_{Si}$ keep constant. Due to the stochastic nature of ion impacts, surface height and composition perturbations $h(x,y,t)$, $\zeta_{Si}(x,y,t)$ and $\zeta_{Fe}(x,y,t)$ are applied to the steady state profile. The perturbations of sputtered atoms flux, to first approximation, write $\delta F_{Si}=FY_{Si}(\zeta_{Si}-c_{Si}\nu_h)$ and $\delta F_{Fe}=FY_{Fe}(\zeta_{Fe}-c_{Fe}\nu_h)$.[25] ν_h

 ©2010 The American Physical Society

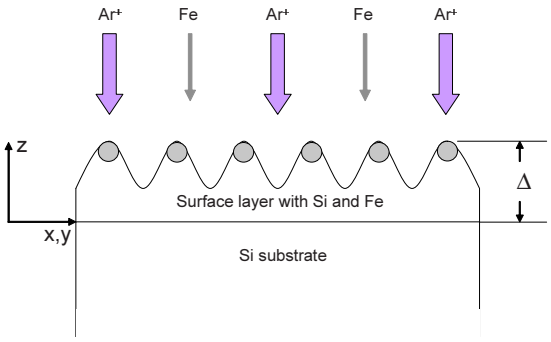

FIG. 1. (Color online) Sketch of a Si (100) surface bombarded by normal incidence Ar^+ ions with Fe codeposition. A surface layer with morphological and compositional modulation is formed during sputtering.

represents the BH instability rising from CDE. At normal incidence, ν_h writes

$$\nu_h = G\nabla^2 h, \tag{1}$$

where G denotes the negative surface tension coefficient.[15] ν_h is assumed to be the same for both species of atoms.[25] Apart from direct ion sputtering, ion-enhanced viscous flow (IVF),[6,26] ballistic smoothing,[27,28] and stress-induced mass transportation[29] are also considered as the relevant surface processes for nanopatterning. IVF, as a long-range mechanism, can be regarded as composition independent and exerts influence only on height evolution as follows:

$$\frac{\partial h}{\partial t} = -F\Omega\frac{\gamma\Delta^3}{\eta_r}\nabla^4 h, \tag{2}$$

where Ω, γ, and η_r denote atomic volume, surface energy, and viscosity,[6] respectively. Ballistic smoothing process as described by

$$\frac{\partial h}{\partial t} = F\Omega\delta\nabla^2 h \tag{3}$$

is also assumed to be identical for both species for simplicity. δ represents the sum of the displacements of recoils.[28] For an undulated surface, a tensile stress induces variation in local chemical potential and then yields surface atomic transportation as follows:

$$J_i = \frac{c_i B_i}{\Omega\Delta} p\,\nabla h, \tag{4}$$

where

$$p = \frac{(1-\nu_s^2)\sigma_0^2}{\gamma E_s} \quad \text{and} \quad B_i = \frac{D_i\rho\Omega^2\gamma}{k_B T}.$$

The subscript i corresponds to Si or Fe. E_s, ν_s, σ_0, D_i, ρ, k_B, and T denote Young's modulus, Poisson ratio, surface stress, diffusivity, areal density of surface mobile atoms, Boltzmann constant, and temperature, respectively.[29,30] p describes the strength of the surface atomic transportation induced by stress, which is positive for tensile stress and negative for compressive stress.[30] It is evidenced that a surface tensile stress could be induced by metal incorporation during ion sputtering of Si surfaces.[29] p is regarded proportional to c_{Fe} with a prefactor being taken as 1 nm^{-1} as a reasonable approximation. This tensile stress-induced surface mass transportation gives rise to a surface instability, which could result in surface modulations by competing other smoothing mechanisms. Taking all these surface processes into account, we obtain two coupled equations for surface height and composition evolution as follows:

$$\Delta\frac{\partial\zeta_{\mathrm{Si}}}{\partial t} = \Omega[(c_{\mathrm{Si}}-1)(\delta F_{\mathrm{Si}} + \nabla\cdot J_{\mathrm{Si}}) + c_{\mathrm{Si}}(\delta F_{\mathrm{Fe}} + \nabla\cdot J_{\mathrm{Fe}})],$$

$$\frac{\partial h}{\partial t} = -\Omega[\delta F_{\mathrm{Si}} + \delta F_{\mathrm{Fe}} + \nabla\cdot J_{\mathrm{Si}} + \nabla\cdot J_{\mathrm{Fe}}] + F\Omega\delta\nabla^2 h - F\Omega\frac{\gamma\Delta^3}{\eta_r}\nabla^4 h. \tag{5}$$

Adopting the definition $H=h/\Delta$, the evolution equations take the form

$$\frac{\partial\zeta_{\mathrm{Si}}}{\partial t} = D\nabla^2 H - C\zeta_{\mathrm{Si}},$$

$$\frac{\partial H}{\partial t} = -A'\nabla^4 H + D'\nabla^2 H + C'\zeta_{\mathrm{Si}}, \tag{6}$$

where

$$C = \frac{F\Omega}{\Delta}Y_{\mathrm{Si}}(c_{\mathrm{Fe}} + c_{\mathrm{Si}}R_Y),$$

$$D = F\Omega Y_{\mathrm{Si}}Gc_{\mathrm{Si}}c_{\mathrm{Fe}}(1-R_Y) + B_{\mathrm{Si}}\frac{p}{\Delta}c_{\mathrm{Si}}c_{\mathrm{Fe}}(R_D-1)$$

$$A' = F\Omega\frac{\gamma\Delta^3}{\eta_r}, \quad C' = \frac{F\Omega}{\Delta}Y_{\mathrm{Si}}(R_Y-1),$$

$$D' = F\Omega Y_{\mathrm{Si}}G(c_{\mathrm{Si}} + c_{\mathrm{Fe}}R_Y) + F\Omega\delta - B_{\mathrm{Si}}\frac{p}{\Delta}(c_{\mathrm{Si}} + R_D c_{\mathrm{Fe}}). \tag{7}$$

R_Y and R_D denote, respectively, the ratios $Y_{\mathrm{Fe}}/Y_{\mathrm{Si}}$ and $D_{\mathrm{Fe}}/D_{\mathrm{Si}}$. In Eq. (6), the nonlinear terms have been omitted for brevity. Since Si concentration is in complementary with Fe in the form $\zeta_{\mathrm{Fe}}=-\zeta_{\mathrm{Si}}$, we just consider the evolution of ζ_{Si}. This model is within the linear regime so that any experimental features related to nonlinear effects are not included here.

III. SIMULATION AND DISCUSSION

A. Dot pattern formation with Fe incorporation

Ion sputtering has been conducted with and without Fe incorporation on two Si (100) samples, denoted as A and B, respectively.[21] The power spectral density (PSD) functions obtained from the atomic force microscopy (AFM) images (inset) of the two samples are given in Fig. 2(a). It shows

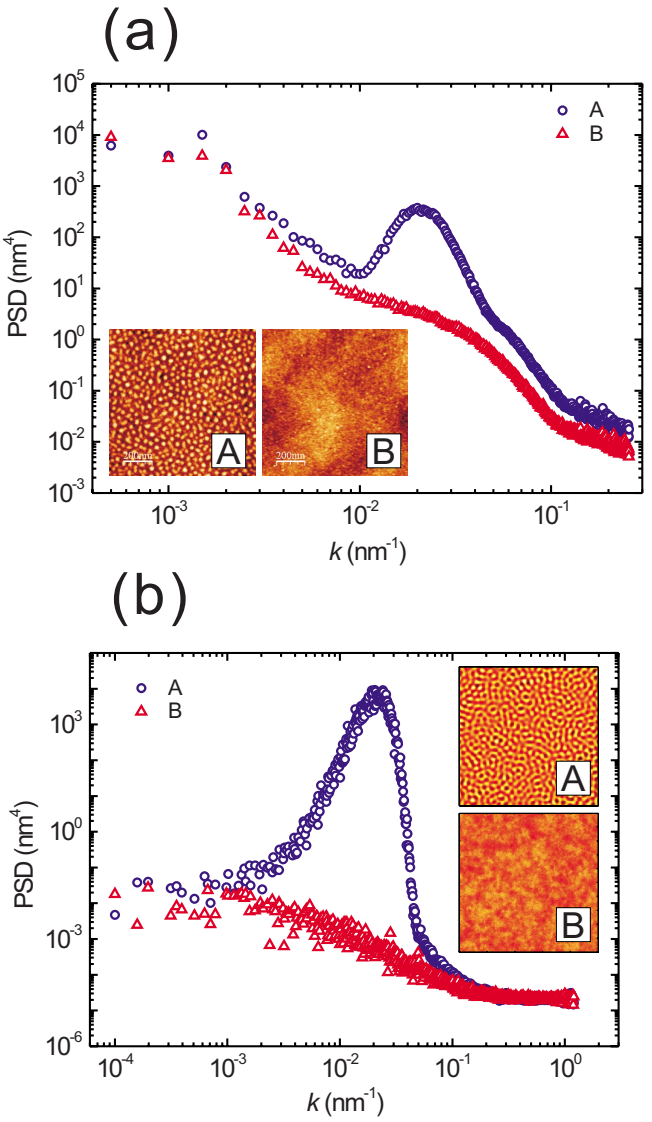

FIG. 2. (Color online) (a) AFM images 1 μm$\times$1 μm (inset) and the corresponding PSD functions from Si (100) surfaces after sputtering in the presence and absence of Fe incorporation (A and B, respectively) (Ref. 21). (b) Simulation of 1 μm$\times$1 μm surface morphologies and the PSD functions.

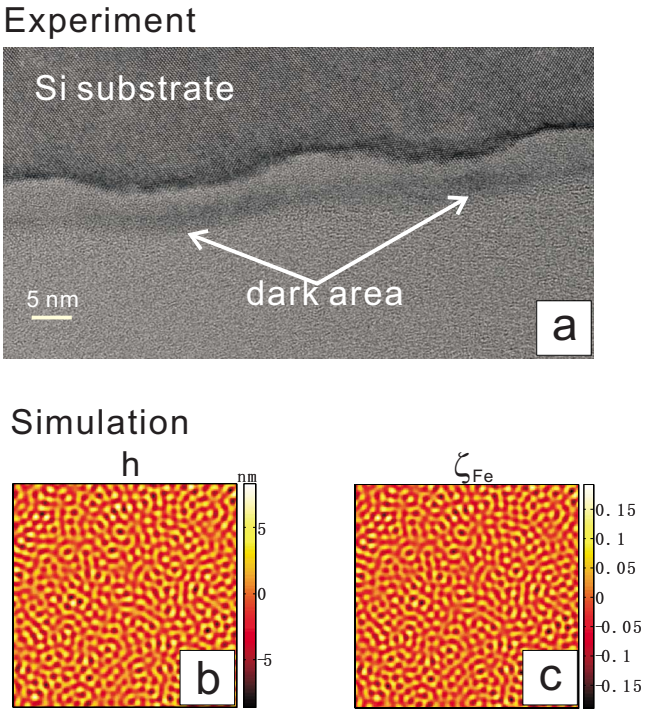

FIG. 3. (Color online) Cross-sectional HRTEM image of the correlated nanodots generated by Fe incorporated ion sputtering (a) (Ref. 21). The simulation results of (b) surface morphology and (c) Fe concentration are both modulated and in phase with each other.

that a nanopatterned surface with a roughness of 0.85 nm is formed on Sample A, which is sputtered with Fe incorporation. In contrast, only a smooth surface with a roughness of 0.23 nm is observed on Sample B, which is sputtered without Fe incorporation. Moreover, a compositional modulation (higher Fe concentration at the top of the dots) is indicated by the cross-sectional high-resolution transmission electron microscopy (HRTEM) image of Sample A [the nanopatterned Si (100) surface] as shown in Fig. 3(a).

Simulation of Si surface evolution during normal incidence 1200 eV Ar^+ ion sputtering with and without Fe incorporation is performed by numerical integration of Eq. (5). The parameters for simulation are listed in Table I. The magnitude of δ scales with ion energy from $\sim$0.1 nm at 100 eV (Ref. 28) to $\sim$1 nm at 1 keV. The energy of incoming Fe atoms (tens of electron volt[20]) is higher than that of the Si atoms on the surface, leading to a higher surface mobility of Fe than Si. However, due to energy transfer by collision, the difference in mobility between Fe and Si could not be very much. Therefore, we take $R_D=2$ as an attempt. The values of B_{Si} and $F\Omega\gamma\Delta^3/\eta_r$ are chosen by making the simulated pattern closest to reality. However, the relative relation between B_{Si} and $F\Omega\gamma\Delta^3/\eta_r$, i.e., $B_{\mathrm{Si}} \gg F\Omega\gamma\Delta^3/\eta_r$,[26] is still satisfied. The finite-difference frequency domain is adopted as the algorithm with system size 250$\times$250, spatial step 4 nm and time step 1 s. c_{Fe} is set to be 0.6 and 0 for Samples A and B, respectively, mimicking Fe incorporation being switched on and off. Additionally, the evanishment of the compositional perturbation in the case of Sample B is represented by $\zeta_{\mathrm{Si}}=0$. After 650 steps of calculation, the morphologies (1 μm$\times$1 μm) of Samples A and B are exhibited in Fig. 2(b) with the corresponding PSD functions. Sample A shows a correlated dot pattern with the periodicity of 45 nm as revealed by the PSD function. The surface roughness is 2.39 nm. In contrast, no pattern is formed on Sample B and the roughness is only 0.0028 nm. It is seen that the surface morphology evolves in a manner resembling that shown in Fig. 2(a). Furthermore, the modulation in Fe concentration [indicated in Fig. 3(a)] is also reproduced by simulation as shown in Fig. 3(c). A close examination of Figs. 3(b) and 3(c) reveals that the modulation in Fe concentration is in phase with that in height, which is consistent with the TEM measurement. The correlation coefficient of surface height and composition is 0.98.

In the above case, the surface instability induced by CDE is overwhelmed by ballistic smoothing, as indicated by $|F\Omega Y_{\mathrm{Si}}G| < F\Omega\delta$ according to Table I. In the absence of Fe,

TABLE I. List of the parameters for simulation.

Category	Parameter	Symbol	Value	Unit
General	Ion flux	F	200	$\mu A/cm^2$
	Sputter yield of Si	Y_{Si}	0.85[a]	
	Ratio of sputter yield	R_Y	0.625[b]	
	Atomic volumn	Ω	0.02	nm^3
	Surface thickness	Δ	2	nm
	Surface energy	γ	10[c]	eV/nm^2
		B_{Si}	3	nm^4/s
BH instability	Ratio of diffusivity	R_D	2	
	BH coefficient	G	−1.04 [d]	nm
IVF	IVF coefficient	$F\Omega\gamma\Delta^3/\eta_r$	25	nm^4/s
Ballistic smoothing	Displacements sum	δ	2.5	nm

[a]Obtained by SRIM 2003.
[b]Reference 31.
[c]Reference 29.
[d]Reference 15.

our model is reduced from a coupled two-field equation to a one-field equation, which resembles the linear theory of BH, as follows:

$$\frac{\partial H}{\partial t} = -A'\nabla^4 H + D'\nabla^2 H, \tag{8}$$

where

$$A' = F\Omega\frac{\gamma\Delta^3}{\eta_r} \quad \text{and} \quad D' = F\Omega Y_{Si}G + F\Omega\delta.$$

The dominance of ballistic smoothing over CDE, expressed as $|F\Omega Y_{Si}G| < F\Omega\delta$, makes D' negative, leading to surface decay over the whole spatial spectrum according to Fourier analysis of Eq. (8). Hence, surface smoothing is observed in the absence of Fe. With Fe being incorporated, preferential sputtering and surface tensile stress come into effect. The tensile stress-induced surface instability works as an essential mechanism for nanopatterning. Together with CDE, this new surface instability overcomes ballistic smoothing (indicated by $|F\Omega Y_{Si}G - B_{Si}p/\Delta| > F\Omega\delta$) and leads to surface modulation. A mathematical analysis reveals that in the absence of the tensile stress, i.e., $p=0$, surface smoothing is still dominant no matter how different Y_{Si} and D_{Si} are from Y_{Fe} and D_{Fe}, indicating that preferential sputtering alone cannot lead to modulation either in morphology or in composition. On the other hand, in the absence of preferential sputtering, i.e., $Y_{Si}=Y_{Fe}$ and $D_{Si}=D_{Fe}$, D and C' equal to zero and Eq. (6) becomes

$$\frac{\partial \zeta_{Si}}{\partial t} = -C\zeta_{Si},$$

$$\frac{\partial H}{\partial t} = -A'\nabla^4 H + D'\nabla^2 H. \tag{9}$$

Although the tensile stress still leads to modulation in surface height, no modulation is generated in composition as ζ_{Si} decays exponentially. Therefore, the tensile stress induces an instability that stimulates modulation in morphology while preferential sputtering cooperating with this instability accomplishes modulation in composition. The rise up of the PSD functions at low frequencies in Fig. 2(a) is attributed to kinetic roughening,[15,29] which is a nonlinear effect and therefore not reproduced in our simulation as a linear approximation.

B. Pattern decaying during postsputtering without Fe incorporation

For further investigation, samples were patterned by ion sputtering with Fe incorporation, and subsequently irradiated without Fe.[21] Figure 4 shows the AFM images of the starting surface (a), and those postsputtered with different fluences (b)–(d), respectively. The evolution of surface roughness obtained from 1 $\mu m \times 1$ μm AFM images and that of the Fe surface content obtained from RBS are shown in Fig. 5(a).

Simulation of this postsputtering experiment is conducted. In this case, c_{Fe} is set evolving with sputtering time in the form like $c_{Fe}=c_{Fe0}\exp(-0.006t)$ so as to mimic the decay of Fe content due to postsputtering without Fe further incorporated. The evolution of c_{Fe} as an exponential decay can be derived from Eq. (6). The coefficient −0.006 is obtained by fitting the experimental result. The other parameters follow Table I. The surface of Sample A as shown in Figs. 2(b), 3(b), and 3(c) is used as the starting surface for postsputtering simulation so that $c_{Fe0}=0.6$. The results are shown in Figs. 4(e)–4(h) and 5(b). The nonmonotonic behavior in roughness evolution as shown experimentally in Fig. 5(a) is reproduced by simulation as depicted in Fig. 5(b). At the beginning of postsputtering Fe atoms inherited from the prepatterning process still remain on the surface although further Fe incorporation is now prevented. Therefore, the tensile stress instability together with CDE is still large enough to compete ballistic smoothing, i.e., $|F\Omega Y_{Si}G - B_{Si}p/\Delta| > F\Omega\delta$, so that the surface modulation keeps growing, as shown by

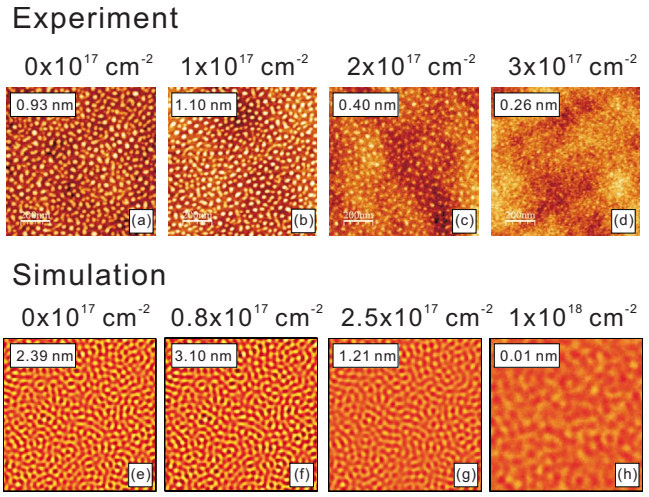

FIG. 4. (Color online) 1 μm $\times$ 1 μm AFM images of Si (100) surfaces prepatterned by 1200 eV Ar^+ ions at normal incidence with Fe incorporation and postsputtered in the absence of Fe at different ion fluences. Surface roughness is shown for each image. [(a)–(d)] Experiment (Ref. 21) and [(e)–(h)] simulation.

Figs. 4(e) and 4(f). With postsputtering proceeding, the incorporated metal atoms are gradually removed from the surface and the smoothing mechanisms dominate the morphology evolution. The smoothing process is also confirmed by Figs. 4(f)–4(h). In this sense, a threshold value of Fe content is expected for the roughening/smoothing transition. When Fe content is greater than this threshold value, the surface instability is large enough to trigger dot pattern formation. Figure 5(b) gives the threshold Fe concentration 0.4, i.e., Fe content $\sim 4 \times 10^{15}$ ions cm^{-2} by adopting the surface layer thickness 2 nm. Experiment also gives a threshold of Fe content, 1×10^{15} ions cm^{-2}.[21] The same order of magnitude of these two threshold values indicates the qualitative agreement between simulation and experiment. The discrepancy might be attributed to pattern growth saturation induced by some nonlinear effects.

C. Further discussion on the continuum model

CDE, IVF, and ballistic smoothing have been regarded by previous studies as the relevant processes during surface nanopatterning induced by ion sputtering.[6,13,26–28] In the presence of Fe incorporation, preferential sputtering, tensile stress-induced surface mass transportation,[29] ion-induced segregation,[32] and the change in collision cascade shape[19] have been proposed as potential mechanisms. Ion-induced segregation explains the nanopatterning process on GaSb.[32] However, in our case, iron silicide has a negative formation enthalpy with respect to Si or Fe simple substance,[33] which implies a tendency of Si-Fe integration for a lower surface energy. Therefore, ion-induced segregation is not applicable here. The change in collision cascade shape that has been used to explain dot/hole transition[19] can be regarded as a high order effect which is not included in our model.

Fick's law diffusion and Mullins diffusion are considered as another two possible surface processes. By integrating these two diffusive terms into our model, we simulate the surface evolution of Si (100) during ion sputtering with or without Fe incorporation. There is no qualitative difference from the numerical results of the model without these two terms, indicating that Fick's law and Mullins diffusion are not dominating mechanisms for Fe motivated ion patterning. However, the integration of Fick's law and Mullins diffusion does improve the simulation as evidenced by a much closer result to experiment, which shows the validity of these two terms.

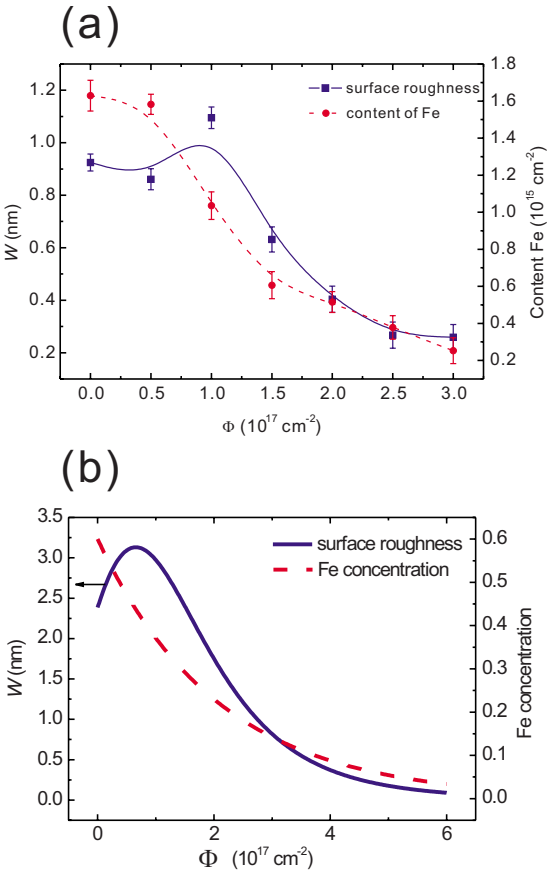

FIG. 5. (Color online) Surface roughness W and Fe content versus fluence Φ during postsputtering of Si (100) surface prepatterned by ion sputtering with Fe incorporation. (a) Experiment (Ref. 21) and (b) simulation.

Since our model is based on a linear equation, some experimental features such as the fine shape of dots, kinetic roughening, and pattern growth saturation cannot be predicted.[15] However, the linear model we developed explains the basic experimental features such as pattern formation in the presence of Fe, surface smoothing in the absence of Fe, and the decaying behavior during postsputtering on prepatterned surfaces. As a first approximation, a linear model is able to describe Fe motivated ion-nanopatterning.

IV. CONCLUSION

We developed a continuum model to describe surface evolution of Si (100) during normal incidence Ar^+ ion sput-

tering with Fe incorporation. The model integrates a number of relevant surface processes, among which surface stress and preferential sputtering are introduced as the effect of Fe incorporation. In this model, the surface stress-induced instability works as origin of patterning in morphology by competing with smoothing mechanisms. Preferential sputtering, cooperating with the surface stress-induced instability, accomplishes patterning in composition. Based on this model, numerical simulations of normal incidence 1200 eV Ar^+ ion sputtering of Si (100) surfaces with or without Fe incorporation and postsputtering on Si (100) surfaces prepatterned by Fe incorporated ion sputtering qualitatively reproduce the experimental results.

ACKNOWLEDGMENTS

This work has been supported by NSFC through Grants No. 60638010 and No. 60776038. The mathematical assistance of W. B. Chen is also acknowledged. We thank K. Ludwig, E. Chason, C. Rodolfo, and S. Le Roy for discussions and suggestions. The support of Jing Zhou by China Scholarship Council through the program No. [2007]3020 is gratefully acknowledged.

*Author to whom correspondence should be addressed; minglu@fudan.ac.cn

[1] W. L. Chan and E. Chason, J. Appl. Phys. **101**, 121301 (2007).
[2] W. L. Chan and E. Chason, Phys. Rev. B **72**, 165418 (2005).
[3] E. Chason, T. M. Mayer, B. K. Kellerman, D. T. McIlroy, and A. J. Howard, Phys. Rev. Lett. **72**, 3040 (1994).
[4] E. Chason, J. Erlebacher, M. J. Aziz, J. A. Floro, and M. B. Sinclair, Nucl. Instrum. Methods Phys. Res. B **178**, 55 (2001).
[5] R. Gago, L. Vazquez, R. Cuerno, M. Varela, C. Ballesteros, and J. M. Albella, Appl. Phys. Lett. **78**, 3316 (2001).
[6] C. C. Umbach, R. L. Headrick, and K. C. Chang, Phys. Rev. Lett. **87**, 246104 (2001).
[7] L. T. Canham, Appl. Phys. Lett. **57**, 1046 (1990).
[8] K. D. Hirschman, L. Tsybeskov, S. P. Duttagupta, and P. M. Fauchet, Nature (London) **384**, 338 (1996).
[9] M. Zacharias, J. Heitmann, R. Scholz, U. Kahler, M. Schmidt, and J. Blasing, Appl. Phys. Lett. **80**, 661 (2002).
[10] J. Erlebacher, M. J. Aziz, E. Chason, M. B. Sinclair, and J. A. Floro, Phys. Rev. Lett. **82**, 2330 (1999).
[11] B. Ziberi, F. Frost, B. Rauschenbach, and T. Hoche, Appl. Phys. Lett. **87**, 033113 (2005).
[12] L. Ling, W. Q. Li, L. J. Qi, M. Lu, X. Yang, and C. X. Gu, Phys. Rev. B **71**, 155329 (2005).
[13] R. M. Bradley and J. M. E. Harper, J. Vac. Sci. Technol. A **6**, 2390 (1988).
[14] R. Cuerno and A. L. Barabasi, Phys. Rev. Lett. **74**, 4746 (1995).
[15] M. A. Makeev, R. Cuerno, and A. L. Barabasi, Nucl. Instrum. Methods Phys. Res. B **197**, 185 (2002).
[16] J. Munoz-Garcia, R. Cuerno, and M. Castro, Phys. Rev. B **78**, 205408 (2008).
[17] G. Ozaydin, A. S. Ozcan, Y. Y. Wang, K. F. Ludwig, Jr., H. Zhou, R. L. Headrick, and D. P. Siddons, Appl. Phys. Lett. **87**, 163104 (2005).
[18] H. Hofsäss and K. Zhang, Appl. Phys. A: Mater. Sci. Process. **92**, 517 (2008).
[19] J. A. Sanchez-Garcia, L. Vazquez, R. Gago, A. Redondo-Cubero, J. M. Albella, and Zs Czigany, Nanotechnology **19**, 355306 (2008).
[20] S. Macko, F. Frost, B. Ziberi, D. F. Foerster, and T. Michely, Nanotechnology **21**, 085301 (2010).
[21] J. Zhou, S. Facsko, M. Lu, and W. Möller, arXiv:1002.1002 (unpublished).
[22] P. Sigmund, J. Mater. Sci. **8**, 1545 (1973).
[23] M. Castro, R. Cuerno, L. Vazquez, and R. Gago, Phys. Rev. Lett. **94**, 016102 (2005).
[24] J. Munoz-Garcia, M. Castro, and R. Cuerno, Phys. Rev. Lett. **96**, 086101 (2006).
[25] V. B. Shenoy, W. L. Chan, and E. Chason, Phys. Rev. Lett. **98**, 256101 (2007).
[26] S. Vauth and S. G. Mayr, Phys. Rev. B **75**, 224107 (2007).
[27] G. Carter and V. Vishnyakov, Phys. Rev. B **54**, 17647 (1996).
[28] M. Moseler, P. Gumbsch, C. Casiraghi, A. C. Ferrari, and J. Robertson, Science **309**, 1545 (2005).
[29] G. Ozaydin, K. F. Ludwig, Jr., H. Zhou, and R. L. Headrick, J. Vac. Sci. Technol. B **26**, 551 (2008).
[30] A. Pimpinelli and J. Villain, *Physics of Crystal Growth* (Cambridge University Press, Cambridge, England, 1999).
[31] G. R. Castro and A. Ballesteros, Surf. Sci. **204**, 415 (1988).
[32] S. Le Roy, E. Søndergård, I. S. Nerbø, M. Kildemo, and M. Plapp, Phys. Rev. B **81**, 161401 (2010).
[33] E. G. Moroni, W. Wolf, J. Hafner, and R. Podloucky, Phys. Rev. B **59**, 12860 (1999).